IEEE Access
Multidisciplinary | Rapid Review | Open Access Journal

Received May 15, 2019, accepted June 22, 2019, date of publication June 27, 2019, date of current version July 17, 2019.

Digital Object Identifier 10.1109/ACCESS.2019.2925388

Analysis and Design of Three-Coil Structure WPT System With Constant Output Current and Voltage for Battery Charging Applications

LIN YANG, XIAOMING LI, SHENG LIU, ZIWEI XU, CHANGSONG CAI, AND PILONG GUO
School of Electrical Engineering and Automation, Wuhan University, Wuhan 430072, China
Corresponding author: Xiaoming Li (xmli@whu.edu.cn)

ABSTRACT Compared with the traditional plug-in charging system, the wireless charging system for battery charging has broad application prospects due to its significant advantages, such as security, convenience, and aesthetics. In practical applications, in order to prolong the battery lifecycles, it is preferred to charge the battery with constant current (CC) and constant voltage (CV) modes. However, since the battery equivalent resistance varies greatly during charging, it is not easy to design a complete charging system owning CC and CV output characteristics. Besides, the equivalent input impedance of the system is preferably resistive to improve efficiency and enhance power transfer capability; therefore, achieving the zero phase angle (ZPA) operation is extremely important. Hence, a novel three-coil structure WPT system is proposed in this paper to solve the above issues. A comprehensive theoretical analysis for the three-coil system to realize the CC and CV charging modes with perfect ZPA operation at two fixed operating frequencies is presented. Furthermore, due to the parasitic losses of passive components and the instability of the dc input voltage, it is unrealistic to achieve accurate and stable CC and CV outputs through the inherent properties of the circuit itself. Consequently, a simple closed-loop controller is introduced into the system to enable the desired CC and CV charging characteristics with zero voltage switching (ZVS) operation by slightly adjusting the operating frequency. Finally, a confirmatory experimental prototype with 4.6-A charging current and 56-V charging voltage is fabricated to confirm the feasibility and validity of the proposed method. The experimental results agree well with the theoretical analysis.

INDEX TERMS Wireless power transfer, constant current (CC), constant voltage (CV), zero phase angle (ZPA), battery.

I. INTRODUCTION

The wireless power transfer technology, which can transfer electrical energy to the load through magnetic field without twisted electrical wires, is undergoing rapid development in recent decades due to its crucial merit of safety, convenience, isolation, etc. This promising technology has been successfully capturing a host of researchers' attention and has been widely used in various practical power transfer applications, including high-power electric vehicles [1]–[3], low-power consumer electronics [4]–[6], and other industrial areas [7]–[9].

In these practical applications, lithium-ion batteries are generally used as the power supply for their excellent performance, such as inherent high energy, long life, low self-discharge rate, and the like. Normally, in order to prolong the battery lifecycles, it is desirable to charge the battery with constant current (CC) and constant voltage (CV) charging modes. The typical charging profile of the battery during charging operation is shown in Fig.1 [10]. Once the battery is connected to the charging system, the CC charging mode with the preset charging current I_{B_P} is first executed, accompanied by a gradual increase in the battery charging voltage. When the charging voltage rises to the preset voltage level U_{B_P}, the CC mode is immediately switched to the CV mode, and then the charging current drops exponentially. Finally, the charging process is terminated once the charging current hits the one-tenth of the preset charging current I_{B_P}. It can be clearly observed that the equivalent resistance of the battery R_B ($R_B = U_B/I_B$, where U_B and I_B indicate the

The associate editor coordinating the review of this manuscript and approving it for publication was Qiquan Qiao.

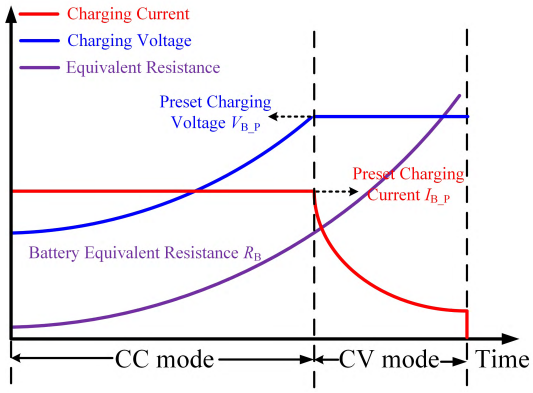

FIGURE 1. Typical charging profile of the Li-ion battery.

real-time charging voltage and current, respectively) varies greatly throughout the whole charging operation. Hence, the implementation of this special charging profile poses a huge challenge to the design of the WPT system.

In order to address the issue mentioned above, a lot of approaches to the WPT system based on control schemes have been presented in the past few years. Control methods for the above-proposed charging problem mainly include three types: phase shift modulation (PSM), frequency conversion control (FCC) and DC-DC converter. Firstly, PSM technology for the high-frequency inverter (HFI) can ensure accurate and constant current or voltage outputs against the time-varying load throughout the entire charging process [11]. However, this universal technology may make it difficult for HFI to achieve zero voltage switching (ZVS) under the significantly variable load condition. Then, the FCC technology is another way to realize the load-independent CC/CV mode charging over the whole charging operation [12]. However, wide range of frequency change is inescapable to cope with the wide range of load variation. This will deprive the system of reliability and stability due to the emergence of frequency bifurcation [13]. Furthermore, it is impossible to realize zero phase angle (ZPA) operation for HFI of the WPT system, and a large circulating current flowing through the system will result in huge power losses. In order to avoid the above-mentioned drawbacks of the PSM and FCC technologies, an extra DC-DC converter (such as Buck, Boost and Buck-Boost circuit) is cascaded at the transmitter or receiver of the WPT system to adjust the charging current or voltage of the battery [14], [15]. However, this method increases the component counts, extra weight/cost and the associated power losses. The three control schemes described above can achieve the desired CC and CV output characteristics, but they are right on the expense of adding the control complexity of the WPT system.

In addition to the above three representative control schemes, quite a few scholars turn their attention to the study of compensation topologies, expecting to realize the requirements of CC and CV charging for the battery, thereby reducing the complexity of control. The authors of [16] conduct a comprehensive and thorough analysis and summary of individual passive resonant networks used to realize ideal load-independent CC or CV output characteristics against the time-varying load. The authors of [17] present a series of higher order compensation topologies for the WPT system that realize stable CC or CV output characteristics with near ZPA and soft switching. The corresponding conclusions in [16], [17] lay a solid foundation for the subsequent research in the field of compensation topology. Based on the above conclusions, the authors in [10] systematically summarize the four basic compensation structures with series-series (SS), series-parallel (SP), parallel-series (PS), and parallel-parallel (PP) topologies for realizing the CC or CV output with the ZPA operation. Besides, two hybrid topologies with the cooperation of SS and PS or the cooperation of SP and PP are presented to achieve the expected battery charging requirement. Moreover, the authors in [18] systematically analyze the three-coil WPT system with a hybrid topology in receiver and two extra switches to realize the CC and CV charging modes with near resistive input impedance. Furthermore, the authors in [19] propose a hybrid topology based on SS and S-LCC compensation, which satisfies the load-independent charging requirement with near zero reactive output of the HFI. However, these approaches mentioned in [10], [17]–[19] have their disadvantages. On the one hand, additional passive components, i.e., inductors and capacitors, as well as several switches composed by two anti-series power MOSFETs with associated driver circuits to switch the hybrid topology, are installed in the system, which not only increase the cost but also increase the volume and weight. On the other hand, accurate CC and CV outputs cannot be obtained by the inherent internal properties of the hybrid compensation due to inevitable parasitic losses in Litz coils and passive components.

To overcome the disadvantages of the control complexity and instability caused by the above-mentioned three control schemes, as well as the drawbacks of the high cost and increased volume/weight caused by the hybrid topology, this paper proposes a novel three-coil structure WPT system to achieve the CC and CV charging modes with the ZPA operation of the HFI at two different operating frequencies, respectively. The designed system can operate at a nearly constant switching frequency in each charging mode, and low loss can be ensured due to the ideal resonant operation throughout the whole charging operation. A detailed design guideline for the designed three-coil structure WPT system is proposed to meet the desired charging profile of the battery. Then, the frequencies for constant current and constant voltage outputs are operated at the CC and CV charging modes, respectively. Furthermore, the mathematical derivation process for the ZPA condition is investigated in detail. In addition, a simple PI closed-loop control scheme is used in the proposed system to maintain the precise charging outputs via only a slight frequency change in each mode.

This paper consists of six sections. A comprehensive theoretical analysis of the load-independent CC and CV output characteristics and the related pure resistive input impedances

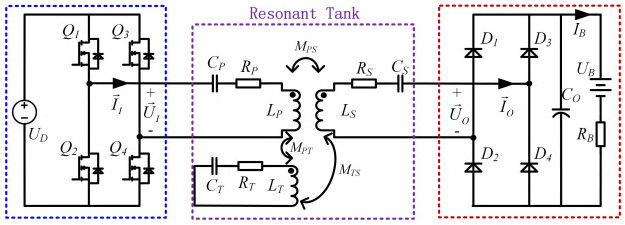

FIGURE 2. Schematic for the proposed three-coil structure WPT system.

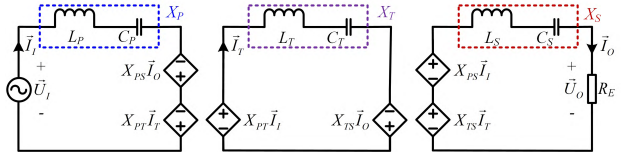

FIGURE 3. Equivalent circuit of the proposed three-coil WPT system.

for each charging mode of the three-coil structure WPT system are presented in Section II. In Section III, parameters design and verification of the presented system for the CC and CV charging modes are described. The design of the closed-loop controller for the CC/CV charging mode is introduced in Section IV. In Section V, an experimental platform is constructed to prove the feasibility and practicality of the proposed method, and the performance of the designed charging system is evaluated by associated experimental results. Finally, some conclusions are drawn in Section VI.

II. THEORETICAL ANALYSIS OF THE THREE-COIL STRUCTURE WPT SYSTEM

A. OVERVIEW OF THE THREE-COIL STRUCTURE WPT SYSTEM AND EQUIVALENT CIRCUIT MODEL

A schematic diagram of the proposed three-coil structure WPT system is depicted in Fig.2. The system consists of an original dc power supply U_D, a full-bridge HFI constituted by four power MOSFETs (Q_1-Q_4), the resonant tank which is comprised of a source coil L_P and a transmitter coil L_T on the transmitter side and a receiver coil L_S on the receiver side as well as their associated series compensation capacitors, a full-bridge uncontrolled rectifier composed of four Schottky diodes (D_1-D_4) and the battery load. Besides, M_{PS} indicates the mutual inductance between the source coil and the receiver coil, M_{PT} represents the mutual inductance between the source coil and the transmitter coil and M_{TS} stands for the mutual inductance between the transmitter coil and the receiver coil.

In order to simplify the analysis of the three-coil structure WPT system, the fundamental harmonic approximation (FHA) is introduced and all of the high-order harmonics are ignored. Moreover, the simplified model of the system is illustrated in Fig.3 for steady-state analysis, where the dc power supply and HFI circuited by blue dashed line and the rectifier and the battery load surrounded by red dashed line in Fig.2 are substituted by an ac voltage source $\vec{U}_I$ and an equivalent resistance $R_E = 8R_E/\pi^2$, respectively [20], [21]. In order to avoid ambiguity, $\vec{U}_I$, $\vec{I}_I$, $\vec{U}_O$, $\vec{I}_O$ and $\vec{I}_T$ are considered as the phasors of the corresponding variables for subsequent analysis. According to the Kirchhoff Voltage Law (KVL), the mathematical relation of the three-coil system can be explicated in (1)

$$\begin{cases} \vec{U}_I = X_P\vec{I}_I - X_{PT}\vec{I}_T - X_{PS}\vec{I}_O \\ 0 = -X_{PT}\vec{I}_I + X_T\vec{I}_T - X_{TS}\vec{I}_O \\ 0 = -X_{PS}\vec{I}_I - X_{TS}\vec{I}_T + (X_S + R_E)\vec{I}_O \end{cases} \tag{1}$$

where $\omega = 2\pi f$ indicates the operating angular frequency under the current working condition; X_P, X_S and X_T represent the equivalent impedances for the three corresponding coil loops, respectively. Besides, X_{PS}, X_{PT} and X_{TS} stand for the equivalent impedances of the three above-mentioned mutual inductances, respectively. Then the related equations can be expressed as

$$\begin{cases} X_P = j\omega L_P + \dfrac{1}{j\omega C_P} \\ X_S = j\omega L_S + \dfrac{1}{j\omega C_S} \\ X_T = j\omega L_T + \dfrac{1}{j\omega C_T} \\ X_{PS} = j\omega M_{PS} \\ X_{PT} = j\omega M_{PT} \\ X_{TS} = j\omega M_{TS} \end{cases} \tag{2}$$

Based on (1), the corresponding voltage and current variables can be calculated as

$$\begin{cases} \vec{I}_I = \dfrac{X_{TS}^2 - X_S X_T - X_T R_E}{A + BR_E}\vec{U}_I \\ \vec{I}_O = -\dfrac{X_{PT}X_{TS} + X_{PS}X_T}{A + BR_E}\vec{U}_I \end{cases} \tag{3}$$

where the symbol A and B in (3) are expressed as follows:

$$\begin{cases} A = X_{TS}^2 X_P + X_{PT}^2 X_S + X_{PS}^2 X_T \\ \qquad + 2X_{PS}X_{PT}X_{TS} - X_P X_S X_T \\ B = X_{PT}^2 - X_P X_T \end{cases} \tag{4}$$

The following analysis of this section focuses on the load-independent CC/CV output characteristics of the proposed three-coil structure WPT system and the related ZPA operation.

B. ANALYSIS OF THE CV CHARGING MODE WITH THE ZPA OPERATION

As described above, the stable CV output regardless of the variable load can be realized by reasonably designing the three-coil structure WPT system. To facilitate analysis, the voltage transfer ratio $E(\omega_{CV})$ is defined as the absolute value of the ratio of the output voltage $\vec{U}_O$ to the input voltage $\vec{U}_I$. According to (3) and the common equation ($\vec{U}_O = \vec{I}_O R_E$), the voltage transfer ratio $E(\omega_{CV})$ can be derived as

$$E(\omega_{CV}) = \left| \frac{(X_{PT}X_{TS} + X_{PS}X_T)R_E}{A + BR_E} \right| \tag{5}$$

Furthermore, it is necessary to derive the equation of input impedance of the system to obtain ZPA condition. Then, combined with the common equation ($Z_I = \vec{U}_I/\vec{I}_I$), the derivation result is as follows:

$$Z_I(\omega_{CV}) = \frac{A + BR_E}{X_{TS}^2 - X_S X_T - X_T R_E} \tag{6}$$

It is obvious from (5) that $E(\omega_{CV})$ is independent of the time-varying load when A in (4) equals to zero. Then, the following equation can be obtained

$$X_{TS}^2 X_P + X_{PT}^2 X_S + X_{PS}^2 X_T + 2X_{PS}X_{PT}X_{TS} - X_P X_S X_T = 0 \tag{7}$$

Clearly, the three coil loops, which are the source loop, transmitter loop and receiver loop, cannot be in resonant state simultaneously due to the invalidation of equation (7) caused by $X_P = X_S = X_T = 0$. For simplicity, three potential solutions are put forward to analyze equation (7), which are illustrated as follows:

Solution one: Assuming that the source coil loop and the transmitter coil loop work in resonant state ($X_P = X_T = 0$) at a specific angular frequency ω_{CV_one}, while the receiver coil loop is in non-resonant state ($X_S \neq 0$). Then, the solution of X_S in (7) can be calculated

$$X_S = -\frac{2X_{PS}X_{TS}}{X_{PT}} \tag{8}$$

Moreover, in combination with the equation (2), the following equation can be obtained

$$\begin{cases} j\omega_{CV\_one}L_P + \dfrac{1}{j\omega_{CV\_one}C_P} = 0 \\ j\omega_{CV\_one}L_T + \dfrac{1}{j\omega_{CV\_one}C_T} = 0 \\ j\omega_{CV\_one}L_S + \dfrac{1}{j\omega_{CV\_one}C_S} = -\dfrac{j2\omega_{CV\_one}M_{PS}M_{TS}}{M_{PT}} \end{cases} \tag{9}$$

Therefore, equation (5) can be simplified to

$$E\left(\omega_{CV\_one}\right)\left|\begin{array}{l} X_P = X_T = 0 \\ X_S = -\dfrac{2X_{PS}X_{TS}}{X_{PT}} \end{array}\right. = \frac{X_{TS}}{X_{PT}} = \frac{M_{TS}}{M_{PT}} \tag{10}$$

It's very intuitive to observe from (10) that if the passive components of the three coil loops are selected to meet the condition in (9), the voltage transfer ratio $E(\omega_{CV\_one})$ is only related to M_{TS} and M_{PT}, which are always constant once the three-coil WPT system is fabricated. In other words, if the input ac voltage $\vec{U}_I$ is constant, the output voltage of the three-coil system maintains unchanged regardless of the variable load at the operating angular frequency ω_{CV_one}.

Moreover, the equation (6) for the input impedance of the system can be further simplified as

$$Z_I(\omega_{CV\_one})\left|\begin{array}{l} X_P = X_T = 0 \\ X_S = -\dfrac{2X_{PS}X_{ST}}{X_{PT}} \end{array}\right. = \frac{X_{PT}^2}{X_{TS}^2}R_E = \frac{M_{PT}^2}{M_{TS}^2}R_E \tag{11}$$

From (11), it is obvious that the equivalent input impedance of the system only has the real component and therefore the three-coil system with solution one can achieve ZPA operation, which avoids a large amount of reactive power dissipation and improves the efficiency and the power transmission capability.

Solution two: Assuming that the transmitter coil loop and the receiver coil loop work in resonant state ($X_T = X_S = 0$) at a specific angular frequency ω_{CV_two}, while the source coil loop is in non-resonant state ($X_P \neq 0$). Then, the solution of X_P in (7) can be derived

$$X_P = -\frac{2X_{PS}X_{PT}}{X_{TS}} \tag{12}$$

Interestingly, the analysis process in solution two is similar to that in solution one described above. Therefore, the detailed derivation process will not be repeated, and the same result can be obtained.

$$\begin{cases} E\left(\omega_{CV\_two}\right)\left|\begin{array}{l} X_T = X_S = 0 \\ X_P = -\dfrac{2X_{PT}X_{PS}}{X_{TS}} \end{array}\right. = \dfrac{X_{TS}}{X_{PT}} \\ Z_I\left(\omega_{CV\_two}\right)\left|\begin{array}{l} X_T = X_S = 0 \\ X_P = -\dfrac{2X_{PT}X_{PS}}{X_{TS}} \end{array}\right. = \dfrac{X_{PT}^2}{X_{TS}^2}R_E \end{cases} \tag{13}$$

As can be seen, both solution one and solution two can achieve load-independent CV output characteristic with ZPA condition at a fixed operating frequency.

Solution three: Assuming that the source coil loop and the receiver coil loop work in resonant state ($X_P = X_S = 0$) at a specific angular frequency ω_{CV_three}, while the transmitter coil loop is in non-resonant state ($X_T \neq 0$). Then, the solution of X_T in (7) can be calculated

$$X_T = -\frac{2X_{PT}X_{TS}}{X_{PS}} \tag{14}$$

Similar to solution one and solution two, the computing results are shown as follows:

$$\begin{cases} E\left(\omega_{CV\_three}\right)\left|\begin{array}{l} X_P = X_S = 0 \\ X_T = -\dfrac{2X_{PT}X_{TS}}{X_{PS}} \end{array}\right. = \dfrac{X_{TS}}{X_{PT}} \\ Z_I\left(\omega_{CV\_three}\right)\left|\begin{array}{l} X_P = X_S = 0 \\ X_T = -\dfrac{2X_{PT}X_{TS}}{X_{PS}} \end{array}\right. = \dfrac{X_{PT}^2 R_E}{X_{TS}^2 - X_T R_E} \end{cases} \tag{15}$$

It can be clearly concluded that the CV output can be obtained at the operating angular frequency ω_{CV_three}. However, the input impedance of the system with solution three needs to be further analyzed. Only when $X_T = 0$ is established, the input impedance Z_I can be treated as a pure resistor. However, it violates the precondition ($X_T \neq 0$). Hence, solution three can only obtain constant voltage output, but cannot realize the ZPA condition.

Detailed comparisons of the three solutions above are listed in TABLE 1. It can be noted that the three solutions have the same voltage transfer ratio, and both solution one and solution two have the same pure resistive input impedance which satisfies the ZPA operation while the input impedance of solution three is not pure resistive. To conclude, solution

TABLE 1. Comparison of the three solutions.

Solution Number	Condition	$E(\omega_{CV})$	$Z_I(\omega_{CV})$	ZPA
Solution One	$X_P = X_T = 0$ and $X_S = -\frac{2X_{PS}X_{TS}}{X_{PT}}$	X_{TS}/X_{PT}	$X_{PT}^2 R_E/X_{TS}^2$	Yes
Solution Two	$X_S = X_T = 0$ and $X_P = -\frac{2X_{PS}X_{PT}}{X_{TS}}$	X_{TS}/X_{PT}	$X_{PT}^2 R_E/X_{TS}^2$	Yes
Solution Three	$X_P = X_S = 0$ and $X_T = -\frac{2X_{PT}X_{TS}}{X_{PS}}$	X_{TS}/X_{PT}	$X_{PT}^2 R_E/(X_{TS}^2 - X_T R_E)$	No

one and solution two can meet the design requirements, while solution three is not feasible.

C. ANALYSIS OF THE CC CHARGING MODE WITH THE ZPA CONDITION

The CC charging mode of the three-coil structure WPT system with the ZPA condition is thoroughly analyzed in this section. To analyze easily, the transconductance gain $G(\omega_{CC})$ is defined as the absolute value of the ratio of the output current $\vec{I}_O$ to the input voltage $\vec{U}_I$. Based on (3), the transconductance gain $G(\omega_{CC})$ can be expressed as

$$G(\omega_{CC}) = \left| \frac{X_{PT}X_{TS} + X_{PS}X_T}{A + BR_E} \right| \tag{16}$$

It can be noted from (16) that $G(\omega_{CC})$ is irrelevant to the variable load when B in (4) is equal to zero at the operating angular frequency ω_{CC}. Then the related equation can be derived

$$X_{PT}^2 - X_P X_T = 0 \tag{17}$$

Hence, the CC charging mode is feasible when (17) is satisfied and the transconductance gain $G(\omega_{CC})$ can be simplified as follows

$$G(\omega_{CC})\Big|_{X_{PT}^2 - X_P X_T = 0} = \left| \frac{X_{PT}X_{TS} + X_{PS}X_T}{X_{TS}^2 X_P + X_{PS}^2 X_T + 2X_{PS}X_{PT}X_{TS}} \right| \tag{18}$$

Based on (3) and (17), the total input impedance of the three-coil system at the operating angular frequency ω_{CC} can be deduced as

$$Z_I(\omega_{CC})\Big|_{X_{PT}^2 - X_P X_T = 0} = \frac{X_{TS}^2 X_P + X_{PS}^2 X_T + 2X_{PS}X_{PT}X_{TS}}{X_{TS}^2 - X_S X_T - X_T R_E} \tag{19}$$

Obviously, the total input impedance does not contain imaginary component when the following equation (20) is satisfied

$$X_{TS}^2 - X_S X_T = 0 \tag{20}$$

Then, the input impedance in the CC charging mode can be further simplified as

$$Z_I(\omega_{CC})\Big|_{\substack{X_{PT}^2 - X_P X_T = 0 \\ X_{TS}^2 - X_S X_T = 0}} = \frac{(X_{PS} + \sqrt{X_P X_S})^2}{R_E} \tag{21}$$

Combined with (20), the equation (18) can be further simplified as

$$G(\omega_{CC})\Big|_{\substack{X_{PT}^2 - X_P X_T = 0 \\ X_{TS}^2 - X_S X_T = 0}} = \left| \frac{1}{X_{PS} + \sqrt{X_P X_S}} \right| \tag{22}$$

According to (21) and (22), the transconductance gain $G(\omega_{CC})$ is independent of the variable load, which indicates that the three-coil WPT system can operate as a constant current source when the input voltage $\vec{U}_I$ is constant. Hence, the CC charging mode can be realized by properly designing the parameters of the three-coil system. Meanwhile, the total input impedance of the three-coil system is pure resistive, which indicates that the ZPA operation can be achieved at a fixed operating angular frequency ω_{CC}. To sum up, the three-coil WPT system can realize expected CC charging with ZPA condition at a fixed operating angular frequency.

III. PARAMETERS DESIGN AND VERIFICATION OF THE PROPOSED SYSTEM FOR THE CC/CV CHARGING MODE

Based on the previous analysis, the three-coil structure WPT system can achieve the desired CC and CV charging characteristics with well-designed parameters at two different operating frequencies, respectively. Besides, both CC and CV charging modes can realize the ZPA operation. However, in the practical design process, it is necessary to use some iteration procedures to determine the parameters of the three-coil system to meet both CC and CV charging requirements with ZPA condition. The detailed flowchart for describing the design process of the system parameters is presented in Fig.4. Firstly, the operating frequency in the CV charging mode f_{CV} is determined in view of the application requirements of the designed system. An operating frequency of 85kHz which meets most application requirement is selected for the CV charging mode in the paper [22]–[24]. Secondly, according to the airgap between transmitter side and receiver side as well as limitation of the installation space, the size of source/receiver coils and coil geometry can be determined. Then, the turns of source/receiver coils and the ferrite volume are initialized to estimate the values of L_P, L_S and M_{PS} by utilizing the magnetic field simulation software such as

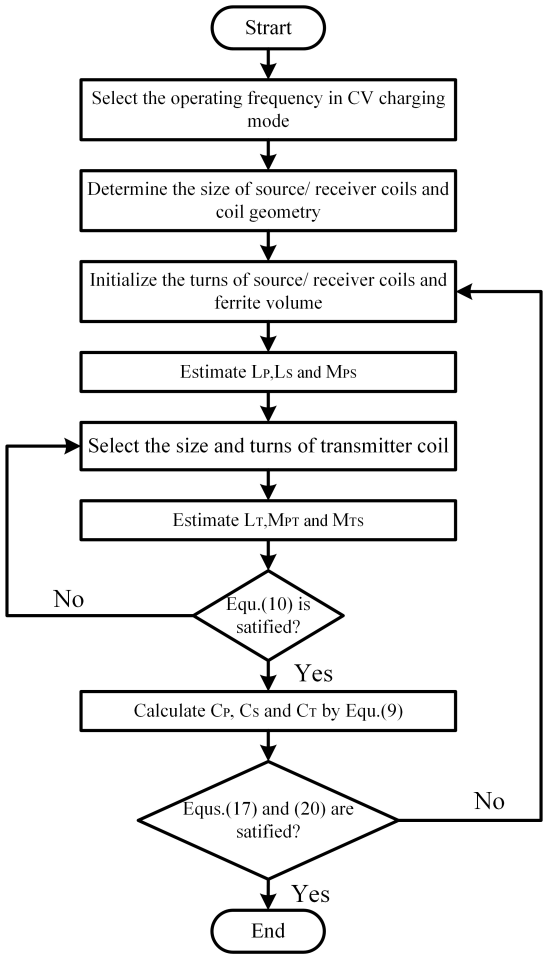

FIGURE 4. Design approaches of the proposed three-coil WPT system.

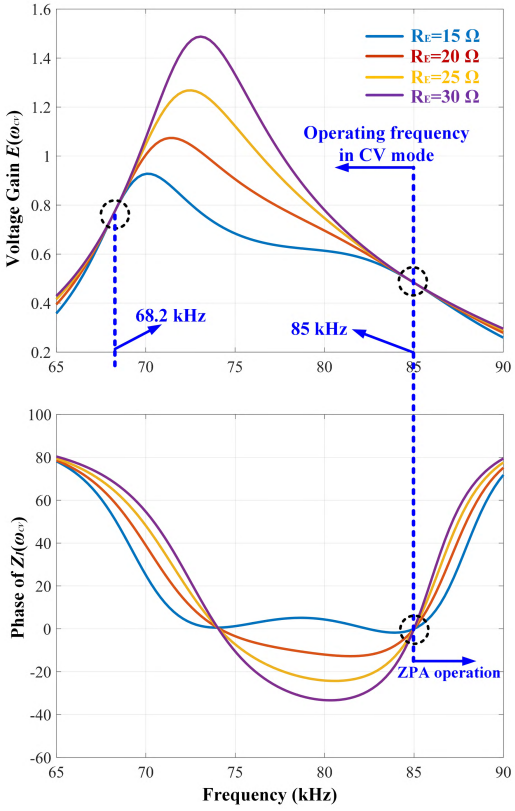

FIGURE 5. Voltage gain and phase of input impedance of the proposed three-coil WPT system.

TABLE 2. Parameters for the designed three-coil WPT system.

Parameter	Designed Value	Measured Value
Self-inductance L_P	128 μH	128.58 μH
Self-inductance L_S	128 μH	128.76 μH
Self-inductance L_S	69 μH	69.15 μH
Resonant capacitance C_P	27.40nF	27.30nF
Resonant capacitance C_S	33.77nF	33.30nF
Resonant capacitance C_T	50.80nF	50.70nF
Mutual inductance M_{PS}	25 μH	25.11 μH
Mutual inductance M_{PT}	30 μH	30.13 μH
Mutual inductance M_{TS}	14.5 μH	14.62 μH
Self-resistances $R_P/R_S/R_T$	0.1/0.1/0.08Ω	0.12/0.12/0.11Ω

JMAG, COMSOL, ANSYS, etc [25], [26]. Moreover, the size and turns of transmitter coil should be selected to estimate the values of L_T, M_{PT} and M_{TS}, which are used to judge whether equation (10) is satisfied or not. Furthermore, the values of C_P, C_S and C_T can be calculated by equation (9). The desired CV charging characteristic and ZPA operation can be achieved with the related parameters calculated above for the three-coil WPT system.

Meanwhile, it is critical to check whether the calculated parameters used in the CV charging mode can also realize the CC charging mode with ZPA condition by utilizing (17) and (20). This cumbersome calculation process can be carried out by mathematical computing software MATLAB. If the verification results satisfy the CC and CV charging characteristics and the associated ZPA operation, the parameters set above are selected for the system design. While, if the parameters calculated in CV mode do not satisfy the equation (17) and (20) in CC mode, then the parameters designed above need to be re-adjusted by varying the turns of coils and the ferrite volume, and the design procedures need to be re-executed.

It is crucial to verify the rationality of the proposed CC/CV charging design method for the three-coil WPT system. All the parameters of the designed three-coil system obtained according to the aforementioned design flow are provided in TABLE 2. The curves of the voltage transfer ratio $E(\omega_{CV})$ and the phase of the related total input impedance $Z_I(\omega_{CV})$ at different loads are drawn as shown in Fig.5. It is clearly observed that there are two frequency points (68.2kHz and 85kHz) that enable the three-coil system to maintain the voltage transfer ratio $E(\omega_{CV})$ unchanged against the variable load. However, the ZPA condition in CV mode can only be obtained at the operating frequency point f_{CV} (85 kHz), but not at the frequency point (68.2kHz). Therefore, the

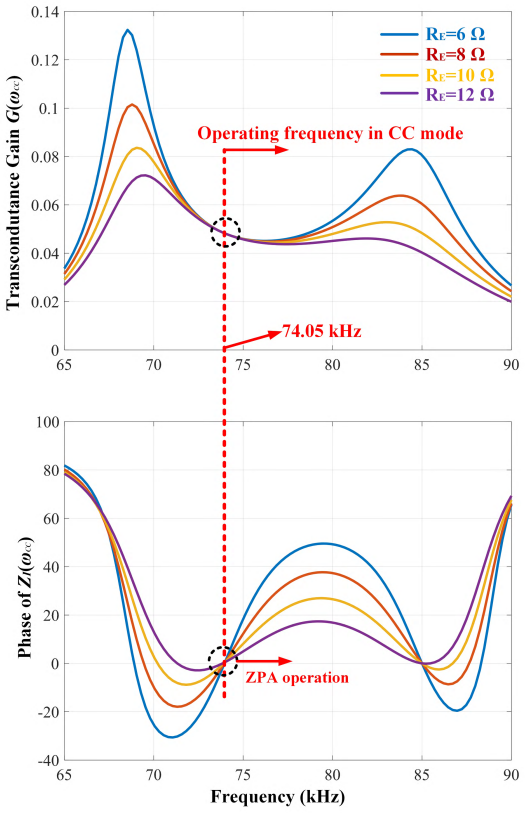

FIGURE 6. Transconductance gain and phase of input impedance of the proposed three-coil WPT system.

frequency point (85kHz) is selected in term of the design requirements. Moreover, the graphs of the transconductance gain $G(\omega_{CC})$ and the phase of the associated input impedance $Z_I(\omega_{CC})$ at different loads are illustrated in Fig.6. It can be noted that both the constant transconductance gain and ZPA condition against the variable load can be achieved at the same frequency point f_{CC} (74.05kHz). Conclusions can be drawn from Fig.5 and Fig.6 that the proposed method can enable the three-coil system to maintain the desired CC and CV output characteristics as well as the associated ZPA operation at two fixed operating frequency points, respectively.

IV. DESIGN OF THE CLOSED-LOOP CONTROLLER FOR THE CC/CV CHARGING MODE

Once the three-coil WPT system is properly designed based on the design procedures mentioned in Fig.4, the CC and CV output characteristics can be readily realized without closed-loop controller at two different operating frequencies, respectively. Besides, the favorable ZPA operation can be obtained in each mode at their respective frequency points. However, due to the parasitic losses of passive components in the circuit, it is unrealistic to achieve accurate CC/CV outputs through the inherent internal characteristics of the circuit itself. Moreover, the dc power supply U_D may be intermittently in a slightly fluctuating state, indirectly causing the charging outputs to be not constant. Therefore, it is necessary to adopt closed-loop control method to maintain

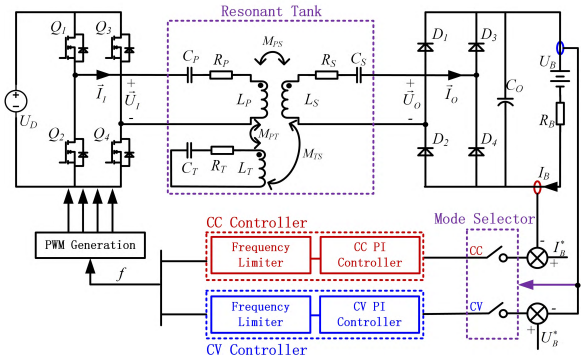

FIGURE 7. Closed-loop control method of proposed three-coil WPT system.

steady charging outputs in each mode and the corresponding ZPA operation.

The closed-loop control method with a simple proportional-integral (PI) algorithm is demonstrated in Fig.7. The adopted closed-loop controller consists of a mode selector, a CC charging controller and a CV charging controller.

The mode selector is specifically configured to select the charging mode according to the demand for charging. If the charging voltage of the battery is below the preset voltage level U_{B_P}, the current controller is activated to perform CC charging output and the voltage controller is deactivated. Conversely, when the charging voltage hits the preset voltage level U_{B_P}, the voltage controller is selected to access the system for the CV charging output and the current controller is turned off. Both the current and voltage controllers consist of a PI control algorithm and a frequency limiter. The frequency limiter is used in the control system to prevent the designed system from operating in a non-ideal frequency range. In CC charging mode, the operating frequency is adjusted slightly above f_{CC}(74.05kHz), and the operating frequency is adjusted slightly above f_{CV} (85kHz) in CV charging mode to make sure that the system always works in the inductive area.

V. EXPERIMENTAL VALIDATION

A. EXPERIMENTAL SETUP

An experimental prototype with 4.6 A charging current in CC charging mode and 56 V charging voltage in CV charging mode based on the schematic in Fig.2 has been set up to verify the correctness of the theoretical analysis mentioned above. The laboratory setup is constructed as shown in Fig.8 and the detailed parameters for the designed three-coil WPT system are provided in TABLE 2. It is worth emphasizing that the experimental setup is used to verify the availability and feasibility of the proposed method. However, in practical applications, the power level and the size of the prototype can be scaled up or down according to the demands of different applications. Four semiconductor switching devices MOSFETs (C2M0080120D) with lower on-resistance are selected to construct the full-bridge HFI. The full-bridge uncontrolled rectifier is built by four fast

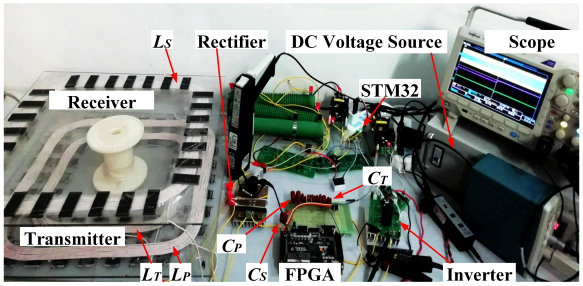

FIGURE 8. Laboratory setup of the proposed three-coil WPT system.

recovery diodes (DSE160-12A) with $V_F = 0.8V$ at rated power. Polypropylene film capacitors are selected in the system for their superior performance such as higher current carrying capacity and lower losses under high-frequency conditions. The FPGA (EP4CE6F17C8N) control unit is applied in transmitter side and the STM32F334C8T6 control unit is in the receiver side. The closed-loop feedback control system for both CC and CV charging modes are implemented with the control unit in transmitter side, the control unit in receiver side is responsible for processing the charging information and feeding back the charging parameters to the transmitter-side control unit through the wireless communication links. The charging voltage and current of the battery are sampled by Hall voltage sensor HVS-AS3.3 and Hall current sensor HCS-ES3.3, respectively.

The square coil structure with rounded corners, which has the advantages of both the square coil structure and the circular coil structure [2], is selected to manufacture the loosely coupled transformer in this study. The Litz wire is extremely suited for manufacturing coils in the WPT field due to its lower skin effect loss and smaller equivalent series resistance under high-frequency conditions. Therefore, the Litz wire (400 strands and diameter of 2.8mm) is utilized for coils design in this paper. The ferrite (PC 40) is applied for enhancing the magnetic coupling. The turns and the size of coils are designed based on the simulation results of JMAG introduced in Section III. Fig.9 shows the designed loosely coupled transformer with a 15cm air-gap distance which is suitable for most application scenarios. The three coils, namely the source coil, the transmitter coil, and the receiver coil, are coaxially symmetrical to increase magnetic coupling between each other. The source coil and the transmitter coil are placed on the same plane to reduce installation space, and the source coil is chosen as the outer coil while the transmitter coil as the inner one. It is worth emphasizing that the coplanar arrangement of the source coil and the transmitter coil is not mandatory, and alternatively, the transmitter coil can be placed between the source coil and the receiver coil. Specifications of the designed source coil, transmitter coil and receiver coil are given in TABLE 3.

Considering the problems mentioned in Section IV, both the presence of parasitic losses in passive components and slight fluctuations in the system's dc input voltage will result in the designed system not being able to accurately implement

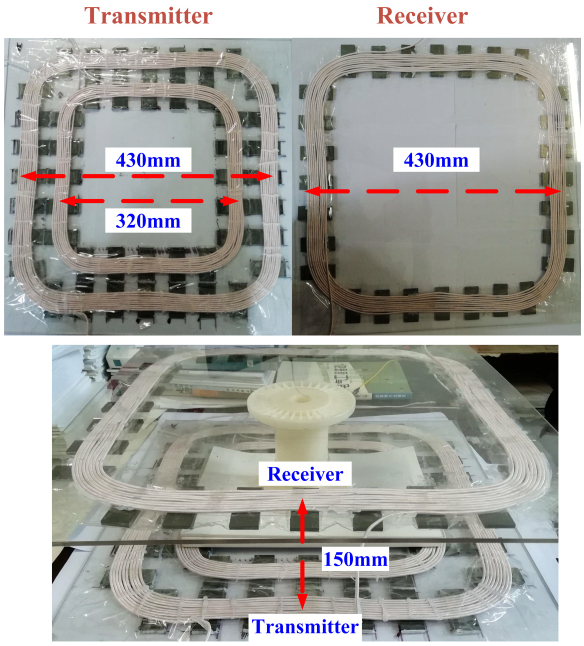

FIGURE 9. Prototype of the constructed coils.

TABLE 3. Specifications of the designed coils.

Parameter	Source Coil	Transmitter Coil	Receiver Coil
Diameter (mm)	430	320	430
Turn (n)	10	10	10

CC or CV charging without closed-loop control. There are two closed-loop methods that can solve the above problems. One is to slightly adjust the phase angle of the HFI to keep the output stable, and the other is to slightly regulate the operating frequency to achieve constant output characteristics. Since the commonly used power switches MOSFETs which are the core components of the HFI have nonnegligible parasitic drain-to-source capacitances, it is desirable to adjust the operating frequency a little bit so that the system is slightly inductive to absolve all the charges of the capacitances before the moment of active turn-on [3]. This is the so-called zero-voltage switching (ZVS). It is difficult to maintain ZVS by phase-shifting control of HFI, while the frequency modulation can easily ensure that the system operates in the inductive region and achieves constant outputs by a slight frequency change in the proposed three-coil system. Therefore, the frequency modulation technology is preferred in this study. The difference between this method and the widely mentioned wide-range frequency modulation technique is that it requires only a little change in the operating frequency to obtain the desired output characteristics.

B. EXPERIMENTAL RESULTS

The output characteristics of the proposed three-coil structure WPT system are verified by experimental tests in this

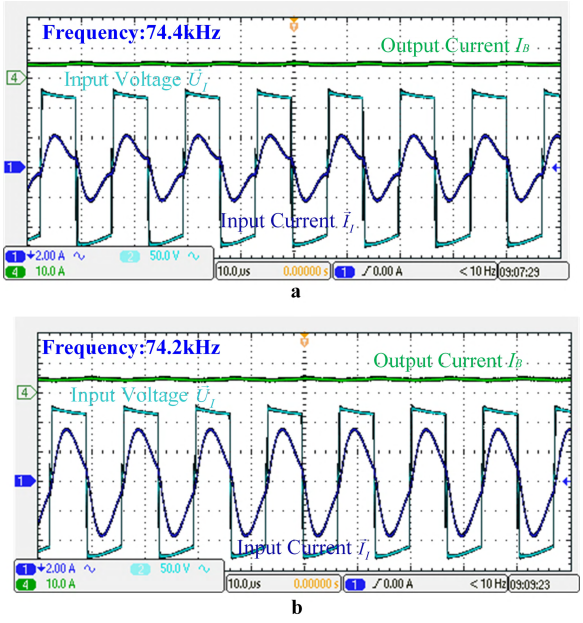

FIGURE 10. Experimental waveforms of I_B, $\dot{U}_I$ and $\dot{I}_I$ in CC charging mode with 120V input. (a) $R_B = 5\ \Omega$. (b) $R_B = 10\ \Omega$.

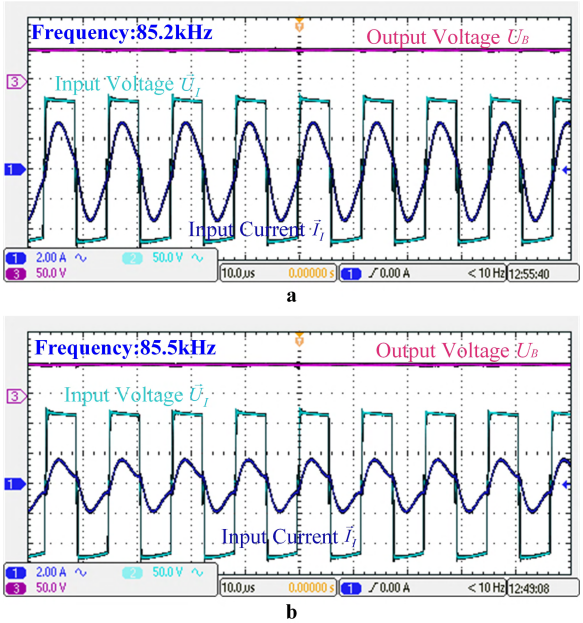

FIGURE 11. Experimental waveforms of U_B, $\dot{U}_I$ and $\dot{I}_I$ in CV charging mode with 120V input. (a) $R_B = 17\ \Omega$. (b) $R_B = 34\ \Omega$.

Section. First, the CC charging mode with a constant dc power source (120V in this paper) at different loads is considered. The experimental waveforms of the output voltage $\vec{U}_I$ and current $\vec{I}_I$ of the HFI and the charging current I_B of the battery are given in Fig.10. Fig.10(a) and Fig.10(b) illustrate the corresponding waveforms at two different loads 5 Ω and 10 Ω, respectively. The charging current I_B in both Fig.10(a) and Fig.10(b) is constant at 4.6 A and the ZVS of the power MOSFET are ideally obtained. Besides, it can be noted that the operating frequencies in Fig.10(a) and Fig.10(b) are 74.4kHz and 74.2kHz, respectively. By comparing Fig.10(a) with Fig.10(b), it can be clearly observed that the CC output characteristics with only a slight frequency variation can be perfectly achieved.

Then, the CV charging mode with a 120V dc input voltage is investigated. Fig.11(a) and Fig.11(b) show the experimental waveforms of $\vec{U}_I$, $\vec{I}_I$ and U_B at two different loads 17 Ω and 34 Ω, respectively. The charging voltage U_B in both figures is constant at 56V and the ZVS of the switches is perfectly achieved. Moreover, it can be obviously observed that switching frequencies in these two figures are 85.2kHz and 85.5kHz, respectively. This strongly proves that the proposed method can achieve a constant voltage output by a little frequency variation.

Furthermore, the experimental waveforms with a 5% increase in input voltage which results in a 126V dc supply in both CC and CV charging modes are depicted in Fig.12. In the CC charging mode shown in Fig.12(a), the charging current is 4.6 A and ZVS is perfectly obtained at the switching frequency 74.5kHz. Besides, in the CV charging mode shown in Fig.12(b), the charging voltage is 56 V and ZVS is ideally achieved at the operating frequency

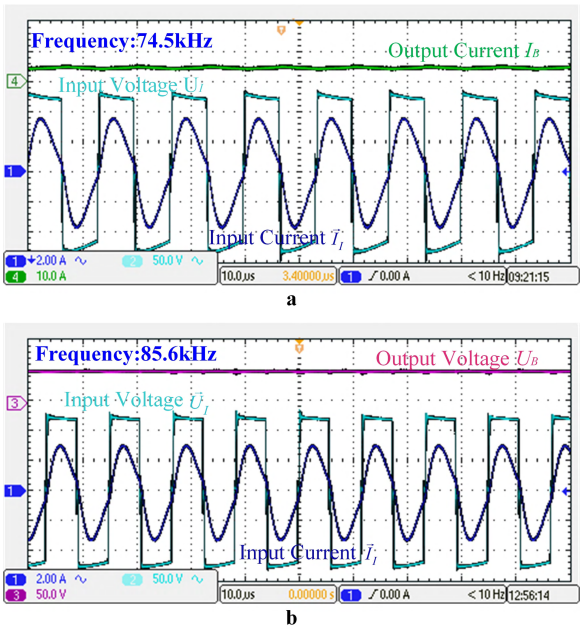

FIGURE 12. Experimental waveforms of U_B, $\dot{U}_I$ and $\dot{I}_I$ with 126V input. (a) $R_B = 10\ \Omega$ in CC charging mode. (b) $R_B = 17\ \Omega$ in CV charging mode.

85.6kHz. From the comparison between Fig.10(b)(Fig.11(a)) and Fig.12(a)(Fig.12(b)), we can get that both the stable CC and CV charging characteristics with ZVS operation can be ensured by varying frequency a little bit even if the input voltage fluctuation is up to 5%.

Fig.13 shows the transient response of CC and CV closed-loop control of the three-coil structure WPT system with 120V dc input voltage. For the CC charging operation,

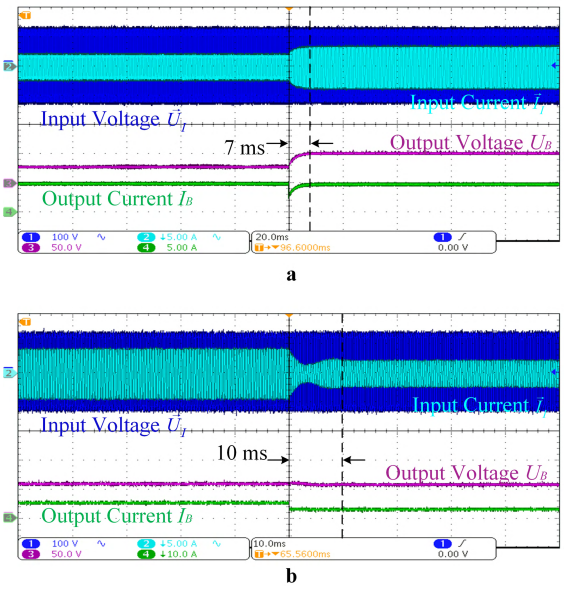

FIGURE 13. Transient response of the CC and CV closed-loop control system. (a) Load change from 10 to 5 Ω in CC charging mode. (b) Load change from 12 to 24 Ω in CV charging mode.

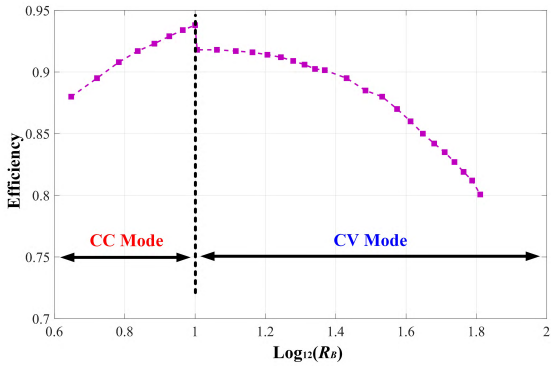

FIGURE 14. Efficiency of the proposed three-coil WPT system in the whole charging process.

the corresponding transient waveforms when load change from 10 Ω to 5 Ω are shown in Fig. 13(a), while the transient waveforms when load has a step change from 12 Ω to 24 Ω for the CV charging operation are shown in Fig.13(b). This control system shows excellent performance with the transient adjustment time of 7 ms in the CC charging mode and that of 10 ms in the CV charging mode.

The experimental charging efficiency (from the dc power supply to the battery load) of the proposed three-coil WPT system versus R_B during the entire charging operation is measured as shown in Fig.14. The efficiency of the system climbs up from 88.1% to the peak of 93.8% in the CC charging mode and then drops to 80.2% at the end of the CV charging mode.

The superior performance of the proposed method is that the system can realize precise CC and CV charging output characteristics at two almost constant operating frequencies over a wide range of load variations, respectively. Besides, the proposed system can achieve high efficiency during the whole charging process due to the nearly ZPA and ZVS operation in both CC and CV charging modes. Consequently, the design of the controller is simple, and the reliability and stability of the designed system can be guaranteed. This promising technology is suitable not only for high-power applications such as electric vehicles but also for low-power applications such as biomedical implants.

VI. CONCLUSION

The focus of this paper is to propose an approach to enable the three-coil structure WPT system to achieve accurate and stable CC and CV charging output characteristics for battery charging applications. The critical feature of the presented three-coil system is that the CC and CV charging outputs with associated ZPA operation can be perfectly obtained at two fixed operating frequencies, respectively. A detailed design methodology, the confirmation of parameters and a simple control method to implement the CC/CV charging are described and explained. The system is unique and novel in that it enables accurate CC and CV charging for the battery at two nearly fixed frequencies, respectively. Therefore, it is quite simple for the design of the controller, and the stability and reliability of the system can be guaranteed. The experimental results verify the excellent performance of the three-coil WPT system, which is consistent with the theoretical predictions.

REFERENCES

[1] F. Liu, K. Chen, Z. Zhao, K. Li, and L. Yuan, "Transmitter-side control of both the CC and CV modes for the wireless EV charging system with the weak communication," *IEEE J. Emerg. Sel. Topics Power Electron.*, vol. 6, no. 2, pp. 955–965, Jun. 2018.

[2] C. Cai, J. Wang, Z. Fang, P. Zhang, M. Hu, J. Zhang, M. Hu, J. Zhang, L. Li, and Z. Lin, "Design and optimization of load-independent magnetic resonant wireless charging system for electric vehicles," *IEEE Access*, vol. 6, pp. 17264–17274, 2018.

[3] Z. Huang, S. C. Wong, and C. K. Tse, "Design of a single-stage inductive-power-transfer converter for efficient EV battery charging," *IEEE Trans. Veh. Technol.*, vol. 66, no. 7, pp. 5808–5821, Jul. 2017.

[4] S. Y. Hui, "Planar wireless charging technology for portable electronic products and Qi," *Proc. IEEE*, vol. 101, no. 6, pp. 1290–1301, Jun. 2013.

[5] X. Liu and S. Y. Hui, "Simulation study and experimental verification of a universal contactless battery charging platform with localized charging features," *IEEE Trans. Power Electron.*, vol. 22, no. 6, pp. 2202–2210, Nov. 2007.

[6] S. Y. R. Hui and W. W. C. Ho, "A new generation of universal contactless battery charging platform for portable consumer electronic equipment," *IEEE Trans. Power Electron.*, vol. 20, no. 3, pp. 620–627, May 2005.

[7] C. Cai, "Resonant wireless charging system design for 110-kV high-voltage transmission line monitoring equipment," *IEEE Trans. Ind. Electron.*, vol. 66, no. 5, pp. 4118–4129, May 2019.

[8] T. Orekan, P. Zhang, and C. Shih, "Analysis, design, and maximum power-efficiency tracking for undersea wireless power transfer," *IEEE J. Emerg. Sel. Topics Power Electron.*, vol. 6, no. 2, pp. 843–854, Jun. 2018.

[9] J. Zhou, B. Zhang, W. Xiao, D. Qiu, and Y. Chen, "Nonlinear parity-time-symmetric model for constant efficiency wireless power transfer: Application to a drone-in-flight wireless charging platform," *IEEE Trans. Ind. Electron.*, vol. 66, no. 5, pp. 4097–4107, May 2019.

[10] X. Qu, H. Han, S.-C. Wong, C. K. Tse, and W. Chen, "Hybrid IPT topologies with constant current or constant voltage output for battery charging applications," *IEEE Trans. Power Electron.*, vol. 30, no. 11, pp. 6329–6337, Nov. 2015.

[11] A. Berger, M. Agostinelli, S. Vesti, J. A. Oliver, J. A. Cobos, and M. Huemer, "A wireless charging system applying phase-shift and amplitude control to maximize efficiency and extractable power," *IEEE Trans. Power Electron.*, vol. 30, no. 11, pp. 6338–6348, Nov. 2015.
[12] N. Liu and T. G. Habetler, "Design of a universal inductive charger for multiple electric vehicle models," *IEEE Trans. Power Electron.*, vol. 30, no. 11, pp. 6378–6390, Nov. 2015.
[13] C.-S. Wang, G. A. Covic, and O. H. Stielau, "Power transfer capability and bifurcation phenomena of loosely coupled inductive power transfer systems," *IEEE Trans. Ind. Electron.*, vol. 51, no. 1, pp. 148–157, Feb. 2004.
[14] Z. Huang, S.-C. Wong, and C. K. Tse, "Control design for optimizing efficiency in inductive power transfer systems," *IEEE Trans. Power Electron.*, vol. 33, no. 5, pp. 4523–4534, May 2018.
[15] H. H. Wu, A. Gilchrist, K. D. Sealy, and D. Bronson, "A high efficiency 5 kW inductive charger for EVs using dual side control," *IEEE Trans. Ind. Informat.*, vol. 8, no. 3, pp. 585–595, Aug. 2012.
[16] W. Zhang and C. C. Mi, "Compensation topologies of high-power wireless power transfer systems," *IEEE Trans. Veh. Technol.*, vol. 65, no. 6, pp. 4768–4778, Jun. 2016.
[17] X. Qu, Y. Jing, H. Han, S.-C. Wong, and C. K. Tse, "Higher order compensation for inductive-power-transfer converters with constant-voltage or constant-current output combating transformer parameter constraints," *IEEE Trans. Power Electron.*, vol. 32, no. 1, pp. 394–405, Jan. 2017.
[18] Y. Li, Q. Xu, T. Lin, J. Hu, Z. He, and R. Mai, "Analysis and design of load-independent output current or output voltage of a three-coil wireless power transfer system," *IEEE Trans. Transport. Electrific.*, vol. 4, no. 2, pp. 364–375, Jun. 2018.
[19] R. Mai, Y. Chen, Y. Li, Y. Zhang, G. Cao, and Z. He, "Inductive power transfer for massive electric bicycles charging based on hybrid topology switching with a single inverter," *IEEE Trans. Power Electron.*, vol. 32, no. 8, pp. 5897–5906, Aug. 2017.
[20] Y. Wang, Y. Yao, X. Liu, D. Xu, and L. Cai, "An LC/S compensation topology and coil design technique for wireless power transfer," *IEEE Trans. Power Electron.*, vol. 33, no. 3, pp. 2007–2025, Mar. 2018.
[21] Y. Yao, Y. Wang, X. Liu, F. Lin, and D. Xu, "A novel parameter tuning method for a double-sidedLCLCompensated WPT system with better comprehensive performance," *IEEE Trans. Power Electron.*, vol. 33, no. 10, pp. 8525–8536, Oct. 2018.
[22] L. Zhao, D. Thrimawithana, and U. K. Madawala, "Hybrid bidirectional wireless EV charging system tolerant to pad misalignment," *IEEE Trans. Ind. Electron.*, vol. 64, no. 9, pp. 7079–7086, Sep. 2017.
[23] F. Lu, H. Zhang, H. Hofmann, W. Su, and C. C. Mi, "A dual-coupled LCC-compensated IPT system with a compact magnetic coupler," *IEEE Trans. Power Electron.*, vol. 33, no. 7, pp. 6391–6402, Jul. 2018.
[24] Y. Li, J. Hu, F. Chen, Z. Li, Z. He, and R. Mai, "Dual-phase-shift control scheme with current-stress and efficiency optimization for wireless power transfer systems," *IEEE Trans. Circuits Syst. I, Reg. Papers*, vol. 65, no. 9, pp. 3110–3121, Sep. 2018.
[25] C. Liu, C. Jiang, J. Song, and K. T. Chau, "An effective sandwiched wireless power transfer system for charging implantable cardiac pacemaker," *IEEE Trans. Ind. Electron.*, vol. 66, no. 5, pp. 4108–4117, May 2019.
[26] R. Mai, Y. Zhang, R. Dai, Y. Chen, and Z. He, "A three-coil inductively power transfer system with constant voltage output," *Energies*, vol. 11, no. 3, p. 673, 2018.

LIN YANG was born in Henan, China, in 1991. He received the B.S. degree from the College of Electrical Engineering and Automation, Henan Normal University, Xinxiang, China, in 2013, and the M.S. degree in control engineering from the Wuhan Institute of Technology, Wuhan, China, in 2016. He is currently pursuing the Ph.D. degree with the College of Electrical Engineering and Automation, Wuhan University, Wuhan.

His current research interests include wireless power transfer and power electronics.

XIAOMING LI received the B.Sc. and M.Sc. degrees in electrical engineering and automation from Wuhan University, Wuhan, China, in 1978 and 1986, respectively, and the Ph.D. degree from the Huazhong University of Science and Technology, Wuhan, in 2000.

He is currently a Professor with the College of Electrical Engineering and Automation, Wuhan University. His research interests include wireless power transfer, power system operation and control, and application of power electronics technology in power systems and smart grid.

SHENG LIU received the B.S. degree from the College of Electrical Engineering and Automation, Wuhan University, Wuhan, China, in 2017, where he is currently pursuing the M.S. degree with the College of Electrical Engineering and Automation.

His current research interest includes wireless power transfer.

ZIWEI XU received the B.S. degree from the College of Energy and Electrical Engineering, Hohai University, Nanjing, China, in 2018. She is currently pursuing the M.S. degree with the College of Electrical Engineering and Automation, Wuhan University, Wuhan, China.

Her current research interest includes wireless power transfer.

CHANGSONG CAI was born in Henan, China, in 1992. He received the B.S. degree in electrical engineering from Tianjin Polytechnic University, Tianjin, China, in 2014, and the M.Eng. degree in electrical engineering from Wuhan University, Wuhan, China, in 2017, where he is currently pursuing the Ph.D. degree in electrical engineering.

His current research interests include applied electromagnetics and power electronics, and wireless power transfer based on magnetic resonance and its industrial applications.

PILONG GUO was born in Hubei, China. He received the B.S. and M.S. degrees in electrical engineering from Three Gorges University, Hubei, in 2010 and 2013, respectively. He is currently pursuing the Ph.D. degree with the College of Electrical Engineering and Automation, Wuhan University, Hubei.

From 2013 to 2017, he was a Lecturer with the Department of Electrical Engineering and New Energy, Three Gorges University. His research interests include power converter modeling and simulation, control theory and application, and wireless power transfer and its industrial applications.